IMPROVEMENT OF THE TECHNOLOGY FOR ARC SPOT WELDING OF OVERLAP JOINTS BASED ON THE RESULTS OF MATHEMATICAL MODELLING

O.V. MAKHNENKO, A.N. TIMOSHENKO, A.F. MUZHICHENKO and **P.V. GONCHAROV**
E.O. Paton Electric Welding Institute, NASU, Kiev, Ukraine

Mathematical modelling of the metal-arc spot welding process was carried out by the thermoplasticity method combined with the finite element method to estimate the possibility of improving the welding technology. Performance of a spot welded joint under static and alternating loads was evaluated based on the data on size of the fusion zone and level of residual stresses within the weld spot zone.

Keywords: *arc spot welding, overlap joints, welded frame structures, strength, mathematical modelling*

The technology for arc spot welding (ASW) is well known and has been applied for a long time to produce fillet and butt joints [1–3]. One of the drawbacks of this technology when joining elements more than 1.5 mm thick is the impossibility of ensuring the quality formation of a welded joint in the vertical position and, hence, its serviceability under the effect of working loads. In this case, the joints of a satisfactory quality can be achieved only by ASW through the holes preliminarily made in external elements, this causing a substantial increase in labour intensity of the work. At the absence of holes, for penetration of the lower element of an overlap joint it is necessary to considerably increase the welding current, whereas this leads to increase in volume of the molten metal and its flow down over the vertical plane, thus violating the quality formation of a weld spot (Figure 1).

Study [4] offers an improved technology for gas-shielded metal-arc spot welding of overlap joints in the vertical position without preliminary punching of holes in the external plate being welded. This technology provides spot welded joints of preset sizes and high quality, which is achieved owing to programming of high-cycle welding heating. Welding cycles provide heating up, penetration (burn-through) of the external plate and subsequent formation of a weld spot. The up-to-date automation level allows programming of the sequence of the welding cycles and performing welding in the automatic or semi-automatic mode. However, experimental selection of parameters of high-cycle welding heating for every combination of materials and thicknesses of the elements to be joined is a labour-consuming process.

This study considers the possibilities of applying mathematical modelling to improve the ASW technology. Modelling of the process was carried out by using the thermoplasticity methods combined with the finite element method. Performance of a spot welded joint under static and alternating loads was estimated on the basis of the data on size of the fusion zone and level of residual stresses within the weld spot zone.

The finite element model was developed to model the overlap ASW process (Figure 2). The use was made of the model of a diffuse welding heat source in 2D axisymmetric statement, for which the specific heat flow has the following distribution:

$$q(x, y) = \frac{2q_{ef}}{\pi^{3/2}} k_x\sqrt{k_y} \exp(-k_x x^2 - k_y(y - y_0)^2),$$

where $q_{ef} = \eta I_w U_a$ is the effective thermal power of the welding heat source; I_w is the welding current; U_a is the arc voltage; η is the efficiency of welding heating; and k_x and k_y are the coefficients of distribution of the thermal power.

Figure 1. Poorly formed weld spot because of flow down of the molten metal over the vertical plane

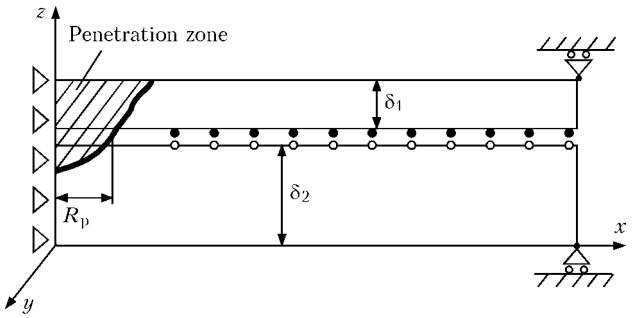

Figure 2. Schematic of finite element model for arc spot welded joint: white and black points — contact elements of surfaces of the upper and lower plates being joined, respectively; δ_1 and δ_2 — thicknesses of the upper and lower plates, respectively

Thermal contact resistance (TCR) between the two plates depends upon the cleanness and roughness of the surfaces, contact pressure and gap between the plates. Therefore, the TCR value may vary within the k_{TCR} = 0.0002–0.0037 W/(mm^2·K) range [5] in each particular case of welding of the plates. However, as shown by the results of calculations with allowance for a short time of the welding process, variation in the TCR values within the above range has no substantial effect on the kinetics of distribution of temperature fields.

In the model developed, variation in TCR between the plates during welding is modelled as follows. If temperature at the contact point at any time step exceeds the melting temperature, at a given time step and at all other steps that follow the k_{TCR} value is equal to the value of heat transfer coefficient at the ideal contact. Therefore, maximal penetration radius R_p between the plates is determined during the process of welding heating. If the contact point is within the penetration zone, at subsequent time steps the k_{TCR} value is equal to the value of heat transfer coefficient at the ideal contact.

Temperature fields in the overlap welded plates in heating and subsequent cooling, as well as a shape and size of the penetration zone are determined as a result of solving the temperature problem. The developed mathematical model describing heating of the overlap welded plates in spatial position on a vertical plane allows for flow out of part of the molten metal during a high-power welding cycle, in which the upper plate is burnt through (Figure 3). Approximate volume of the molten metal that flowed out can be determined on the basis of experimental data.

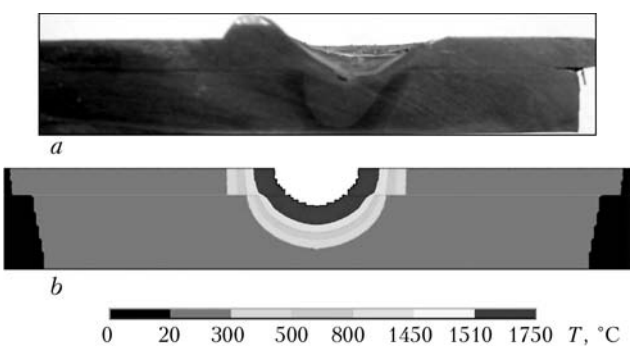

Figure 3. Macrosection of spot welded joint (*a*) and mathematical model that allows for flow out of part of the molten metal after the burn-through welding cycle (*b*)

Table 1. Physical-mechanical properties of steel 09G2S*

T, °C	Thermal conductivity coefficient λ, W/(mm·°C)	Volume enthalpy h_V, J/mm^3	Young modulus $E\cdot10^{-5}$, MPa	Linear thermal expansion coefficient $\alpha\cdot10^5$, 1/°C	Yield stress σ_y, MPa
20	0.040	0	1.97	1.14	435
100	0.040	0.5	1.97	1.14	398
200	0.039	1.0	2.01	1.22	360
300	0.038	1.5	1.95	1.26	323
400	0.036	1.7	1.88	1.30	285
500	0.034	2.0	1.80	1.38	222
600	0.032	2.4	1.69	1.39	97
700	0.029	3.2	1.56	1.41	45
800	0.026	4.0	1.35	1.83	43
900	0.026	5.0	1.25	1.87	43
1000	0.028	6.0	1.25	1.94	43
1100	0.029	7.6	1.25	1.95	43
1200	0.030	9.2	1.25	1.95	43
1400	0.030	10.0	1.25	1.95	43
1510	0.030	15.0	1.25	1.95	43
1750	0.030	17.5	1.25	1.95	43

*Poisson's ratio ν = 0.3.

The temperature and mechanical problems were traced sequentially in time from the beginning of heating to complete cooling of metal. The distribution of temperatures at each time step was used as a load to solve the mechanical problem on evaluation of the stress-strain state at a current time step, allowing for the state at the previous step.

The thermoplasticity problem was solved by using the Prandtl–Reuss theory of plastic flow associated with the Mises yield condition. At each tracing step the linearised problem was solved by the finite element method. Physical non-linearity was realised by the iteration way. The calculation model accounted for the temperature dependence of physical-mechanical properties of steel 09G2S elements (Table 1). To solve the mechanical problem, the finite elements within the penetration zone were fixed to each other, thus modelling fusion of the plates.

The model developed was used to investigate the process of formation of an overlap spot welded joint between two plates of steel 09G2S, 2.5 and 7.0 mm thick, in CO_2 ASW under the conditions consisting of five sequential welding cycles (Table 2, Figure 4). Welding was performed in a spatial position on the vertical plane, this involving certain difficulties with formation of a welded joint.

Table 2. ASW parameters

No. of welding cycle	Arc voltage U_a, V	Welding current I_w, A	Welding wire feed speed v_{feed}, m/h	Welding pulse duration t_w, s	Duration of pause between pulses t_{pause}, s
1	28	200	120	0.4–0.5	0.1
2	42	450	276	1.0–1.3	2.0
3	30	250	138	0.8–1.0	1.5
4	30	250	138	0.8–1.0	1.0
5	26	190	120	0.5	–

The efficiency of welding heating was chosen to be $\eta = 0.7$, based on the data of study [6], as well as on the condition of matching of size of the penetration zone on macrosection of the spot welded joint and calculation results (Figure 5). Thermal power distribution coefficient $k_x = 3.0\ 1/mm^2$ was also corrected on the same condition. Adding a filler material was not modelled in the first heating up welding cycle because of its very short duration and subsequent flow out of the molten metal during the second welding cycle. Volume of the molten metal that flowed out during the second welding cycle was determined from the condition of subsequent filling up with the filler material during the third and fourth welding cycles.

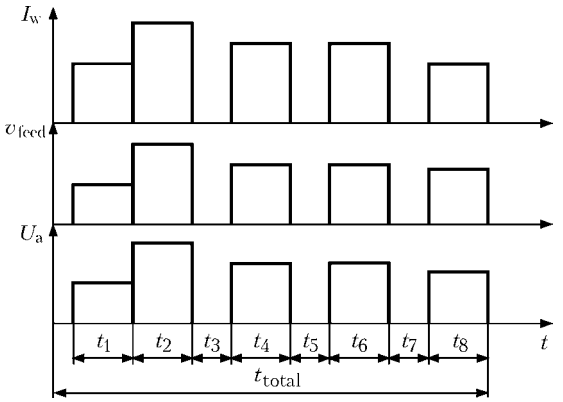

Figure 4. Scheme of variations in parameters of ASW in vertical position: t_1–t_8 — durations of pulses and pauses; t_{total} — total time of ASW cycle

Comparison of the calculation and experimental results shows that the developed mathematical model is adequate for evaluation of formation of the overlap spot welded joint between two plates in ASW in a spatial position on the vertical plane and can be applied to develop the technology for welding such joints with a complex welding cycle.

This mathematical model allowed obtaining the calculation results on the distribution of residual stresses within the welded joint zone. This information can be helpful for estimation of strength of the spot welded joints.

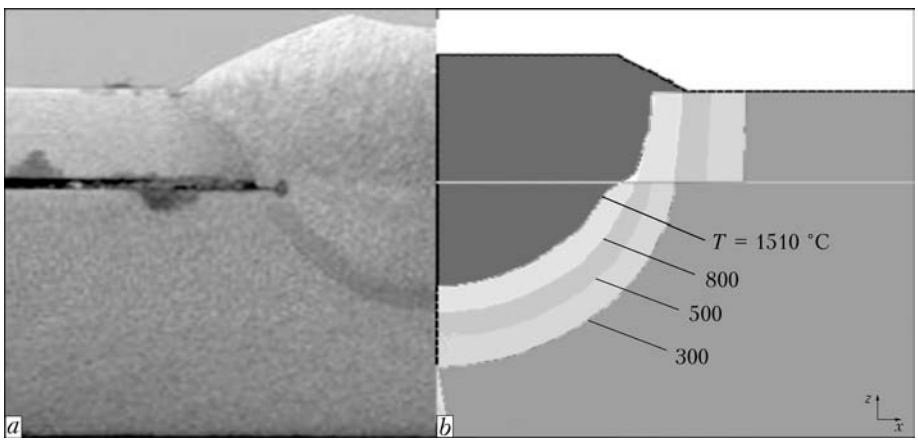

Figure 5. Comparison of size of the penetration zone on macrosection of the spot welded joint (*a*) and calculation results (*b*)

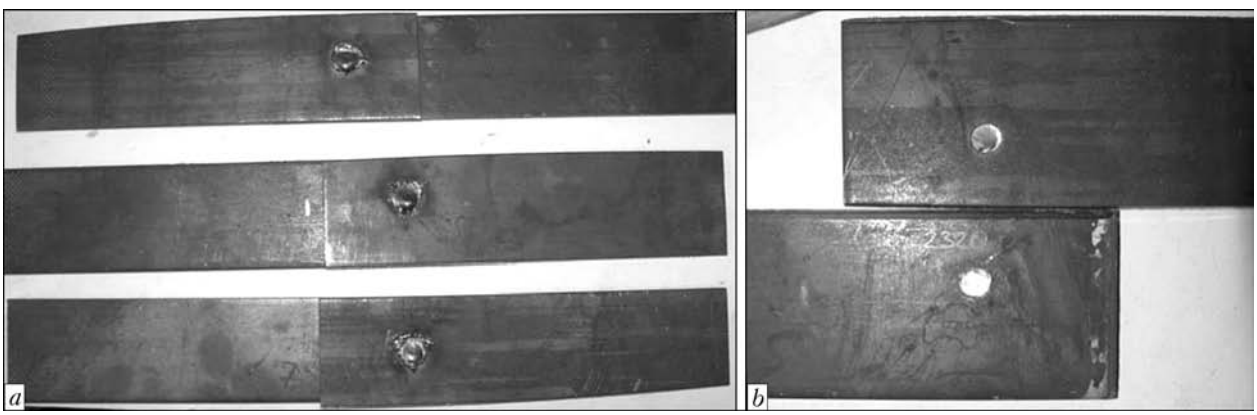

Figure 6. Appearance of samples of spot welded joints before tensile tests (*a*) and after fracture of the weld spots by shear mechanism (*b*)

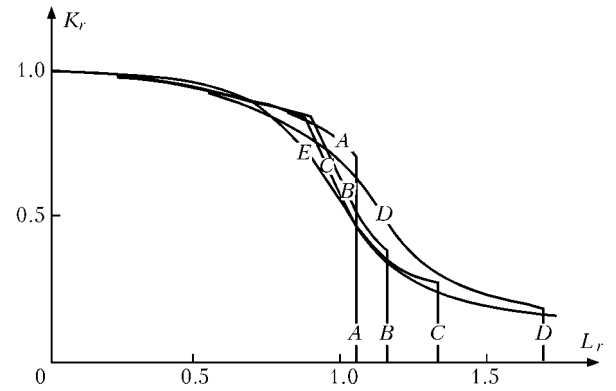

Figure 7. Diagrams of limiting state $K_r \le f_1(L_r)$ for different types of structural steels [3]: *A* — high-strength steel EN408; *B* — pressure vessel steel A533B; *C* — low-carbon steel containing manganese; *D* — austenitic steel; *E* — calculation curve [9]

Welded joints with the spot welds usually fail at fracture of the weld spots by the shear mechanism (Figure 6) [7, 8]. There may be other mechanisms of fracture of the joints both in base metal and HAZ, and because of tear out of a weld spot from the base metal on its perimeter. The determining factor is the fracture that begins at the top of a cavity adjoining the weld spot and propagates either in the bulk of the spot or in the base metal. Therefore, the fracture is initiated by a sharp stress raiser located on the weld spot perimeter. The effect of this raiser can be taken into account on the basis of up-to-date criteria of fracture mechanics, namely the two-parameter criterion of tough-brittle fracture [9, 10]. According to this approach, equilibrium of a crack is not violated, provided that the following condition is met:

$$K_r \le f_1(L_r),$$

where $K_r = K_I / K_{Ic}$ is the ratio of stress intensity factor K_I at the crack apex to the critical value of this parameter K_{Ic}; and $L_r = \sigma_{ref} / \sigma_y$ is the ratio of critical stress σ_{ref} in the weld spot zone that determines fracture by the plastic instability mechanism to yield stress σ_y of the material. The kind of function $f_1(L_r)$ is determined experimentally. Figure 7 gives these data for different structural steels.

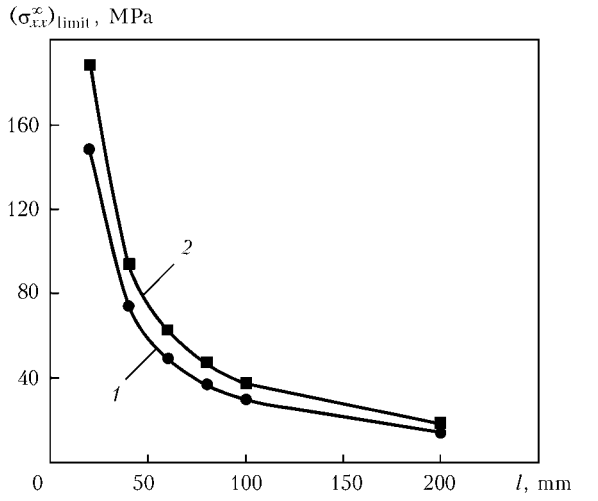

Figure 9. Calculation data on variations in limiting values of stresses $(\sigma^{\infty}_{xx})_{limit}$ in the upper, thinner plate (δ_1 = 2.5 mm, δ_2 = 7.0 mm) under static loading depending on step l of the weld spots $2R$ = = 10 mm in size (shear fracture): *1* — here and in Figures 10 and 11, K_{Ic} = 1025; *2* — 2050 MPa·mm$^{1/2}$

To calculate K_I, it is necessary to account for both external load, i.e. load by force P_x on one spot in plane of the plates welded (Figure 8), and residual non-relaxed stresses within the welded joint zone. When calculating L_r, residual stresses are ignored, as they relax completely.

The P_x values are determined from stresses σ^{∞}_{xx} on the periphery of the elements being joined (Figure 8, *a*), and from values of metal thickness δ_j and step l between the weld spots, i.e. $P_x = \sigma^{\infty}_{xx}\delta_j l$ (j = 1, 2). Loading results in deformation of the joint (Figure 8, *b*). In deformation, the weld spot is affected by shear force $P_x = P_x \cos\beta$, tear force $P_z = P_x \sin\beta$, and momentum

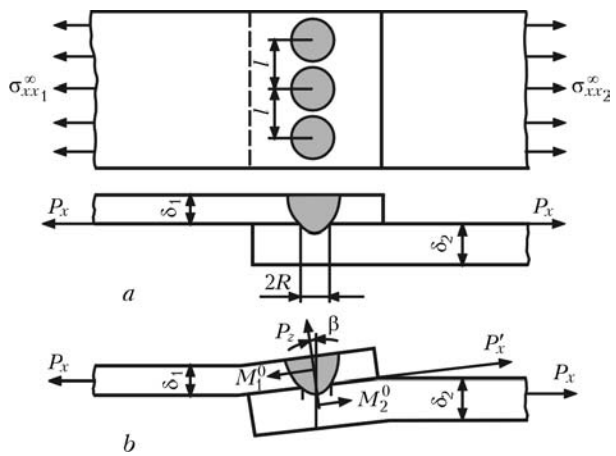

Figure 8. Schematics of welded joint with a single-row weld before loading (*a*) and its deformation at P_x (*b*): l — distance between the weld spot centres (step); P'_x — force acting within the weld spot zone; M^0_1 and M^0_2 — forces acting on the upper and lower plates being joined, respectively; β — bend angle

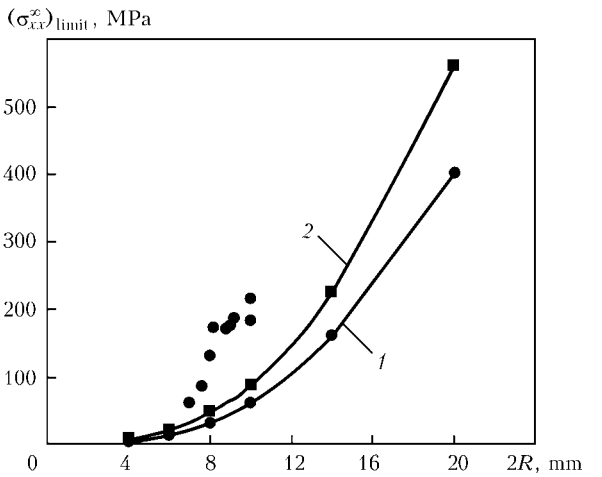

Figure 10. Comparison of calculation (*1*, *2*) and experimental data (points) of limiting values of stresses $(\sigma^{\infty}_{xx})_{limit}$ in the upper, thinner plate (δ_1 = 2.5 mm, δ_2 = 7.0 mm) under static loading depending on size $2R$ of the weld spot with step l = 50 mm

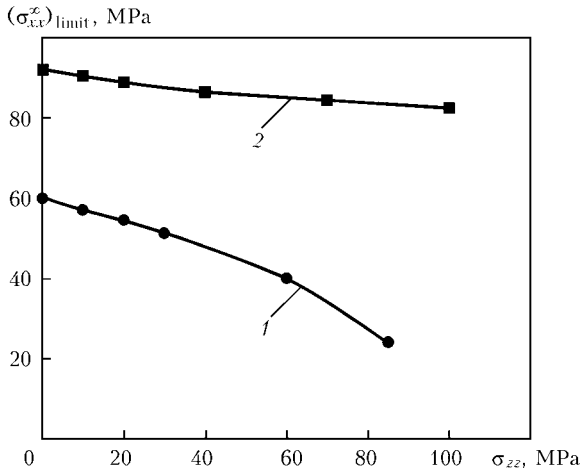

Figure 11. Variations in limiting values of stresses $(\sigma^{\infty}_{xx})_{limit}$ in the upper plate (δ_1 = 2.5 mm, δ_2 = 7.0 mm) under static loading depending on residual stresses σ_{zz} (weld spot size $2R$ = 10 mm, l = = 50 mm)

$$M = M_1^0 + M_2^0 = P_x \frac{\delta_1 + \delta_2}{2} \cos \beta.$$

The values of angle β are in a complex dependence upon the geometric parameters of the welded joint, mechanical properties of the materials and force P_x. Parameters of deformation of the overlap spot welded joint and values of K_I can be calculated from the relationships suggested in studies [11, 12]. The said relationships were used to calculate the limiting values of stresses $(\sigma^{\infty}_{xx})_{limit}$ in the upper, thinner plate under static loading depending on step l of the weld spots $2R$ in size, thicknesses of the upper and lower plates, δ_1 and δ_2, respectively, and residual stresses σ_{zz} within the weld spot zone.

The calculation data given in Figure 9 show that the limiting values of stresses $(\sigma^{\infty}_{xx})_{limit}$ under static loading dramatically decrease with increase in step l of the weld spots.

Size of a weld spot also has a substantial effect on the limiting values of stresses $(\sigma^{\infty}_{xx})_{limit}$ (Figure 10). Increase in size of the weld spot leads to increase in strength of the welded joint under static loading. Comparison of the calculation and experimental data in Figure 10 shows that the applied calculation approach is sufficiently conservative.

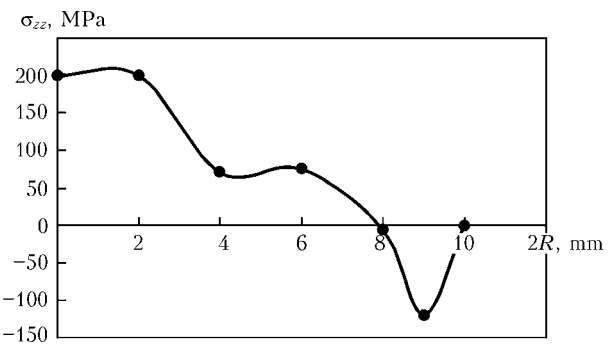

Figure 12. Calculation data on distribution of residual stresses σ_{zz} within the weld spot zone along the fusion line of the plates welded (δ_1 = 2.5 mm, δ_2 = 7.0 mm, weld spot size $2R$ = 10 mm)

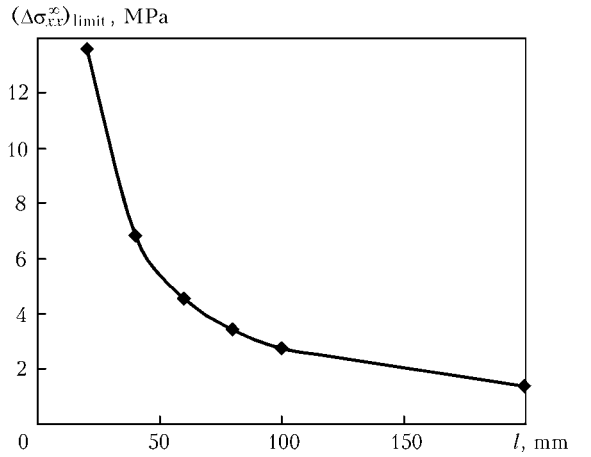

Figure 13. Variations in limiting values of stress range $(\Delta\sigma^{\infty}_{xx})_{limit}$ in the upper, thinner plate (δ_1 = 2.5 mm, δ_2 = 7.0 mm) under cyclic loading on a base of $2 \cdot 10^6$ cycle depending on step l of the weld spot $2R$ = 10 mm in size (shear fracture)

Increase in thickness of both upper and lower plates has a negative effect on strength of the spot welded joint. This factor is negative for the improved ASW technology with high-cycle welding heating, which is used primarily for welding of rather thick plates.

The calculation data in Figure 11 show that the effect of the level of residual stresses σ_{zz} acting through thickness of the plates within the weld spot zone on the limiting values of stresses $(\sigma^{\infty}_{xx})_{limit}$ in the upper, thinner plate under static loading is negligible. As seen from Figure 12, the level of residual stresses σ_{zz} is fairly low. According to the equilibrium equation, the integral of normal stresses σ_{zz} along the fusion line (area) should be equal to zero. This gives grounds to state that the level of residual stresses is not a determining factor for strength of the spot welded joints under static loading.

The limiting state condition for cyclic loading of the spot welded joints can be formulated as follows [13]:

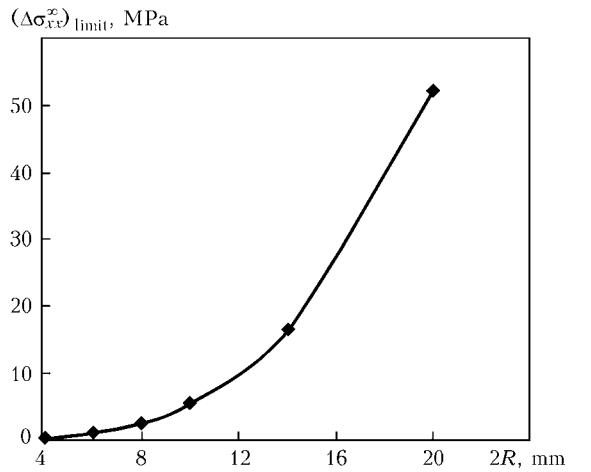

Figure 14. Variations in limiting values of stress range $(\Delta\sigma^{\infty}_{xx})_{limit}$ in the upper, thinner plate (δ_1 = 2.5 mm, δ_2 = 7.0 mm) under cyclic loading on a base of $2 \cdot 10^6$ cycle depending on weld spot size $2R$ at l = 50 mm

$$\Delta K_{\omega^*}^{\max} = K_{\omega^*}^{\max} - K_{\omega^*}^{\min} = \Delta K_{\text{th}}^{0}(1 - \alpha r_\sigma),$$

where the maximal and minimal values $K_{\omega^*}^{\max}$ and $K_{\omega^*}^{\min}$ are determined at $P_x = P_x^{\max}$ and $P_x = P_x^{\min}$, respectively; r_σ is the coefficient of asymmetry of the cycle of variation in force P_x; ΔK_{th}^0 is the threshold value of a range of stress intensity factor K_{I} ($r_\sigma = 0$), at which a normal tear crack does not practically propagate; and α is the experimental characteristic of the material ($\alpha \approx 0.50$–0.85) [13].

Strength of the spot welded joint under cyclic loading was calculated depending on step l and size $2R$ of a weld spot, as well as thickness of the upper and lower plates, δ_1 and δ_2, respectively, at a conservative value of cycle asymmetry coefficient $r_\sigma = 0$ and $\Delta k_{\text{th}}^0 = 190$ MPa·mm$^{1/2}$. As seen from the calculation data shown in Figures 13 and 14, this dependence is of the same character as under static loading. However, as to the limiting values, the stress range under cyclic loading on a base of $2 \cdot 10^6$ cycle is approximately an order of magnitude lower (at a level of 10–20 MPa) than under static loading, this being in agreement with the up-to-date notions of cyclic strength of the welded joints.

CONCLUSIONS

1. High-quality spot welded joints can be provided by regulating parameters of welding cycles in ASW of thin-sheet metal in vertical position. The improved technology offers new possibilities for applying ASW for fabrication of structures in different industries, in particular for fabrication of frame structures of modern freight and passenger railway cars.

2. The developed mathematical model can be efficiently used to develop the technologies for overlap ASW, including with complex welding cycles.

3. As shown by the calculation data, the level of residual stresses σ_{zz} acting through thickness of the plates within the weld spot zone is rather low. According to the equilibrium equation, the integral of normal stresses σ_{zz} along the fusion line (area) is equal to zero. Therefore, the level of residual stresses is not a determining factor for strength of the spot welded joints under static loading.

4. The limiting values of stresses $(\sigma_{xx}^{\infty})_{\text{limit}}$ under static loading and stress range $(\Delta\sigma_{xx}^{\infty})_{\text{limit}}$ under cyclic loading dramatically decrease with increase in step of the weld spots.

5. Increase in size of the weld spot leads to a substantial increase in strength of the welded joint both under static and cyclic loading.

1. Tereshchenko, V.I., Sharovolsky, A.N., Sidorenko, K.A. et al. (1983) Peculiarities of CO_2 metal-arc spot welding. *Avtomatich. Svarka*, **9**, 51–53.
2. Tkachenko, A.N., Voskresensky, A.S. (2005) Application of arc spot welding in fabrication of car bodies. *The Paton Welding J.*, **12**, 22–24.
3. *GOST 14776–79*: Arc welding. Spot welded joints. Main types, design elements and sizes. Introd. 01.07.80.
4. Lobanov, L.M., Timoshenko, A.N., Goncharov, P.V. (2009) Arc spot welding of overlap joints in vertical position. *The Paton Welding J.*, **1**, 26–28.
5. Lienhard, J. et al. (2002) *Heat transfer textbook*. Cambridge, Massachusetts: Phlogiston Press.
6. Rykalin, N.N. (1951) *Calculations of thermal processes in welding*. Moscow: Mashgiz.
7. Dorofeev, A.N. (1964) *Calculation of strength of spot welds*. Moscow: Mashinostroenie.
8. Serenko, A.I., Krumboldt, M.N., Bagryansky, K.V. (1977) *Calculation of welded joints and structures*. Kyiv: Vyshcha Shkola.
9. Harrison, R.P., Looscmore, K., Milne, J. et al. (1980) Assessment of the integrity of structure containing defects. *Central Electricity Generating Board Rep. 6, Rev. 2*. Berkley.
10. Makhnenko, V.I., Pochinok, V.E. (1982) Application of fracture mechanics criteria in calculation of strength of welded joints with specified discontinuities of the crack-like type. *Avtomatich. Svarka*, **1**, 1–6.
11. Makhnenko, V.I., Ryabchuk, T.G., Pochinok, V.E. (1990) Improvement of the strength design procedure for spot welded joints. *Ibid.*, **1**, 9–14.
12. Cherepanov, G.P. (1974) *Brittle fracture mechanics*. Moscow: Nauka.
13. Makhnenko, V.I., Pochinok, V.E. (1984) Cyclic loads resistance of welded joints with incomplete penetration welds. *Avtomatich. Svarka*, **10**, 33–40.